



## PAPER

## OPEN ACCESS

RECEIVED  
26 October 2020REVISED  
26 January 2021ACCEPTED FOR PUBLICATION  
3 February 2021PUBLISHED  
10 February 2021

Original content from this work may be used under the terms of the [Creative Commons Attribution 4.0 licence](#).

Any further distribution of this work must maintain attribution to the author(s) and the title of the work, journal citation and DOI.



## Layered double hydroxides intercalated with methyl orange as a controlled-release corrosion inhibitor for iron in chloride media

N Bakhtaoui<sup>1,2</sup>, O Benali<sup>2</sup>, E Mazarío<sup>3</sup>, Francisco J Recio<sup>3</sup> and P Herrasti<sup>3</sup><sup>1</sup> University of Abou Bekr Belkaid Tlemcen Chemistry Department, Faculty of Science, Algeria<sup>2</sup> Laboratory of Chemistry: synthesis, proprieties and applications, University Dr Moulay Tahar, Saïda, Algeria<sup>3</sup> Universidad Autónoma de Madrid, Facultad de Ciencias. Dept. Química Física Aplicada. 28049 Madrid. SpainE-mail: [javier.recioc@uam.es](mailto:javier.recioc@uam.es) and [pilar.herrasti@uam.es](mailto:pilar.herrasti@uam.es)**Keywords:** layered double hydroxide, methyl orange, inhibitor, corrosion

## Abstract

In this study, the corrosion inhibition properties of nanocontainer-type layered double hydroxide (LDH) are evaluated on iron that is immersed in a 3.5% NaCl aqueous solution. LDH ZnAl-NO<sub>3</sub> was synthesized via coprecipitation. The material presents satisfactory crystallinity with a Zn/Al ratio of 2:1. Methyl orange (MO) has been added into the synthesis process by exchange with nitrate ions and/or by adsorption of MO onto LDH surfaces (LDH-MO). Iron was immersed in solutions with various concentrations of LDH and LDH-MO ranged 1–6 g l<sup>-1</sup>, and the corrosion inhibition properties were investigated using linear sweep voltammetry, electrochemical impedance spectroscopy (EIS), and SEM. Based on pitting potential studies, LDH has demonstrated inhibition of the pitting corrosion process, and the optimal concentration was identified as 2 g l<sup>-1</sup>. The presence of MO in LDH provides excellent anticorrosive properties with a mixed inhibition mechanism. The corrosion potential of LDH-MO presents more noble values and exchange current densities that are one order of magnitude less than those of the bare iron after 72 h of immersion in a 3.5% NaCl aqueous solution. EIS results corroborated that the corrosion resistance increased when 2 g l<sup>-1</sup> of LDH-MO was in solution. SEM images support the anticorrosive behaviour of the LDH-MO.

## 1. Introduction

Corrosion is a great problem in society, especially in metals in contact with seawater. This is due to the strong corrosion that metals suffer in this environment by the presence of chlorides. One solution is the use of polymer coatings, this is the most widespread method to prevent the metallic structures exposed to aggressive media. The coating acts as a physical barrier against the aggressive environment. However, for a long time proposes, the use of polymer coating is not enough barrier for corrosion protection. The aging and the presence of defects in the polymer coating create channels, which expose the metal surface to the aggressive media. Besides, polymer coatings exposed to aqueous media develop conductive pathways for the diffusion of corrosive species through the coating to the metallic surface [1]. Both situations increase the probability to develop the corrosion process. The ways to mitigate these problems are the use of cathodic protection or the addition of corrosion inhibitors in the polymer coatings. The addition of inhibitors in polymer coating needs to be controlled since the direct addition of inhibitors to the coating could decrease the inhibitor efficiency deteriorating the polymer matrix, and lost the anticorrosive properties before to the exposition to the aggressive media [2]. For this reason, in recent years, many studies have focused on using compounds with ‘self-healing’ properties [3]. These materials can host inhibitors and that they can be released to the environment only if necessary. Among them, microcapsule [4] nanocontainers [5], mesoporous silica [6, 7], Halloysite nanotubes [8, 9] and LDH [3, 10, 11]

Layered double hydroxides (LDHs) are composed of ‘brucite-like’ cationic layers, where the inclusion of trivalent cations introduces an overall positive charge to the nanosheets. The formula is  $[M^{2+}_x M^{3+}_{1-x} (OH)_2]^{x+} (A^{n-})_{x/n} \cdot mH_2O$  where  $M^{2+}$  and  $M^{3+}$  are divalent and trivalent lamellar metal cations, respectively,  $A^{n-}$  is interlayer anion to balance the electrical charge of the structure. In synthetic materials, the

relative proportions of di and trivalent cations can vary and  $x$  generally takes values between 0.20 and 0.33. The variation of the stoichiometric coefficient and the exchange of anionic species hosted in the interlayer of the LDH compounds give to these structures different properties and applications [12–17]. In the past decade, the use of LDHs as nanocontainers for corrosion protection has been an important task due to the anion-ex-change aptitude [3, 10, 11, 18–21]. This property can be exploited using these nanocontainers as a host for corrosion inhibitors between the interlayer and their release on demand when some changes in the interface are produced, such as change of pHs, presence of corrosive species, for example, chloride. A lot of effort has been devoted to the generation of LDH compounds for the prevention of active metal corrosion. The focus has been performed on aluminium and magnesium alloys [22–25] since the LDH can grow directly with the surface ions, but recently the studies have been extended to zinc, steel and carbon steel [26, 27]. Many anions have been chosen to intercalate into the LDH as inorganic  $\text{NO}_2^-$ ,  $\text{CrO}_4^-$ , [27], and organics, all of them with effective corrosion protection [28].

In recent studies, a great variety of inhibitors such as mercaptobenzothiazolate [21], fatty acid [29], nitrite, phosphate and molybdate [30–33] were located into the LDH gallery and their active corrosion protection properties were examined. In addition, new hybrid heterostructures as different silane-LDH have been explored improving the corrosion inhibition [16, 31].

Another interesting property of LDH compounds is the adsorption of azo dyes in wastewater by the exchange properties of the azo dyes [34–37]. Azo dyes are also employed as corrosion inhibitors in acid media due to the good adsorption on the metallic surface [38–40].

In this work, the LDH compounds containing nitrate and methylene orange are used in solution to study the corrosion inhibition effect on iron in chloride media simulating seawater. To our knowledge, the reuse as a corrosion inhibitor of LDH previously employed to remove methyl orange (LDH-MO) it has not been studied. Through this research, it is expected two advantages, the elimination of a dye (MO) from the medium and the use of this compound as a corrosion inhibitor.

## 2. Experimental

### 2.1. Synthesis of layered double hydroxides (LDHs) and LDH-methyl orange (LDH-MO)

The  $\text{M}^{2+}:\text{M}^{3+}$  ratio that was chosen for the synthesis of the LDHs in this study was 2:1 to obtain stable layered compounds. A conventional coprecipitation method was used to synthesize Zn–Al– $\text{NO}_3$  LDHs [21, 41]. A mixed solution ( $V = 50$  ml) of 0.5 M  $\text{Zn}(\text{NO}_3)_2 \cdot 6\text{H}_2\text{O}$  and 0.25 M  $\text{Al}(\text{NO}_3)_3 \cdot 9\text{H}_2\text{O}$  was added dropwise into 1.5 M  $\text{NaNO}_3$  solution ( $V = 100$  ml and  $\text{pH} = 10$ ) under vigorous stirring at room temperature. During this reaction, the pH of the solution was maintained at 10 via the addition of a 2 M NaOH solution. The obtained white product was subjected to hydrothermal treatment without stirring at 65 °C for 24 h for crystallization of the LDHs. Afterward, the product was centrifuged and washed four times with distilled water before being dried at 50 °C for 24 h. All processes were conducted under an atmosphere of nitrogen to prevent impurities such as  $\text{CO}_3^{2-}$ . The product was labelled LDH.

Methyl orange (MO), which was intercalated with LDHs, was prepared using the ion-exchange method. In a typical reaction, 0.32 g of MO was dissolved in 100 ml of distilled water; into this solution, two other solutions were added dropwise, one that contained 50 ml of LDHs (1 g), and the other 1 M NaOH (100 ml). Both solutions were added at the same time (adding dropwise of the two solutions takes 1 h). The addition was conducted at a constant pH of 9 under a nitrogen atmosphere and vigorous stirring. This stirring was completed after 24 h after addition of all compounds at room temperature. The resulting precipitate was washed four times with distilled water, centrifuged, and dried at 65 °C for 24 h. The final product was denoted as LDH-MO.

### 2.2. Characterization of the LDH compound

X-ray diffractograms were recorded between 2° and 65°  $2\theta$  in an X'pert PRO-theta/2theta Panalytical diffractometer that was equipped with an X'Celerator rapid detector with Cu K $\alpha$  radiation ( $\lambda = 1.5406$  Å) at room temperature. The values of basal spacing was calculated by the Bragg equation.

SEM images were obtained using a Hitachi 3000N microscope and used to determine the morphologies of the synthesized samples and the metal after specified time in the 3.5% NaCl solution and in the 3.5% NaCl solution containing LDH or LDH-MO. The microscope is equipped with an Quantax EDS analyzer, model XFlash 6130, from Bruker to determine the atomic ratio between Zn and Al.

### 2.3. Electrochemical characterization

A three-electrode cell was used with a gold electrode as the auxiliary electrode, Ag/AgCl/KCl (sat) as the reference electrode and iron metal with a purity of 99% as the working electrode. The exposed area of this electrode was 2 cm<sup>2</sup>. Cyclic voltammetry and polarization curves were measured at 5 mVs<sup>-1</sup> with an Autolab 30

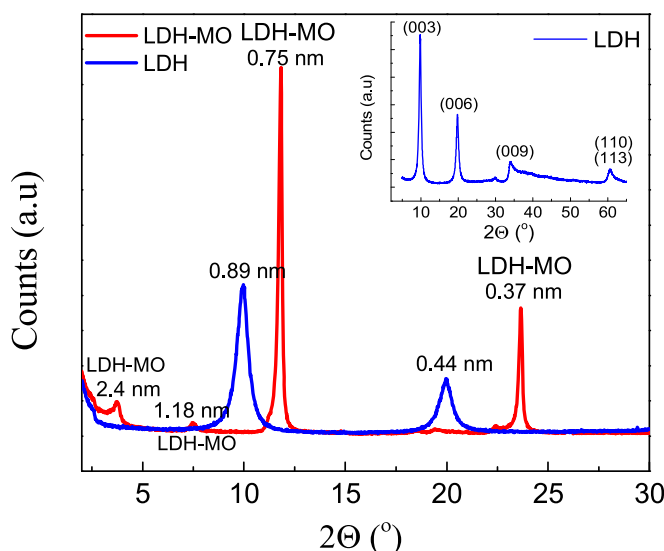


**Figure 1.** XRD patterns of LDH and LDH-MO. Inset corresponds to the diffractogram at high values of  $2\theta$ .

potentiostat. The electrochemical measurements were conducted in an aggressive medium (3.5% NaCl in distilled water) and a non-aggressive medium (Britton-Robinson buffer solution, adjusted to pH 7 with NaOH). The iron species were immersed in solutions with LDH at various concentrations ranged from 1 to  $6 \text{ g l}^{-1}$  and in solution with LDH-MO at the same concentrations. To investigate the anticorrosive properties, the pitting potential ( $E_{\text{pit}}$ ) was determined from the linear sweep voltammetry test performed from the open circuit potential ( $E_{\text{oc}}$ ) to  $\pm 300 \text{ mV}$  versus  $E_{\text{ocp}}$ . The cathodic and anodic polarizations have been performed with independent samples, and the electrochemical behaviours in the aggressive versus non-aggressive media were compared. The  $E_{\text{pit}}$  values were regarded as the potential when the current density increased one order of magnitude from the baseline of the voltammetry results for iron in the non-aggressive medium. The exchange current density ( $i_0$ ) and the corrosion potential ( $E_{\text{corr}}$ ) were calculated by extrapolating the Tafel slopes (anodic and cathodic) determine from the polarization curves.

EIS analysis was performed on iron ( $2 \text{ cm}^2$ ) for 2 h of immersion times in 3.5% NaCl solution and adding LDH and LDH-MO in a  $2 \text{ g l}^{-1}$  concentration. The measurements were implemented at OCP using 10 mV perturbation in the frequency range of 10 KHz–10 mHz.

### 3. Results and discussion

The XRD patterns that are presented in figure 1 depict a good crystallinity with symmetric and intense peaks at low  $2\theta$  values corresponding to (003), (006) and (009) reflections and less intense peaks at higher  $2\theta$  values with clear (110) (113) reflections. The reflections a low  $2\theta$  correspond to 0.89, 0.44 and 0.31 nm, respectively, indicating that LDH has a good ordering along the stacking direction and also has the structure of brucite layers due to the relation  $d_{003} = 2d_{006} = 3d_{009}$ . The (110) and (113) reflections were observed at  $2\theta = 60.8^\circ$  that were typical of materials such as LDHs.

In the x-ray diffraction of LDH-MO, three new harmonic peaks appear at  $2\theta$  positions of  $3.7^\circ$ ,  $7.4^\circ$  and  $11.8^\circ$  corresponding to d-values of 2.4, 1.18 and 0.75 nm, respectively. These new peaks are ascribed to the (003), (006) and (009) reflections due to MO<sup>−</sup> anions intercalated in the interlayer LDH host [42]. The expansion of the basal interlayer distance ( $d_{003}$ ) of the host LDH lattice from 0.89 to 2.40 nm, which parallels the MO intercalation, points toward the successful exchange with  $\text{NO}_3^-$  anions [43]. The diffractogram at higher values of  $2\theta$  for the LDH-MO was not modified.

SEM images of the LDH and LDH-MO and EDS results are presented in figures 2(a) and (b). The LDH product consists of agglomerates with crystalline structures, and the EDS analysis shows that the atomic ratio of Zn to Al is close to 2. When MO was incorporated, the morphology was similar, but the structural definition was lower. This could be associated with the presence of MO not only in the interlamellar space but also on the LDH surface via electrostatic interaction. For LDH, the relation between Zn and Al, remains unaltered, and the presence of carbon, oxygen, and sulfur is detected due to the presence of MO.

The inhibition corrosion properties of the LDH were evaluated by considering the pitting potential ( $E_{\text{pit}}$ ), which was expressed as the potential at  $j = 0.001 \text{ A cm}^{-2}$  (this current density is one order of magnitude higher

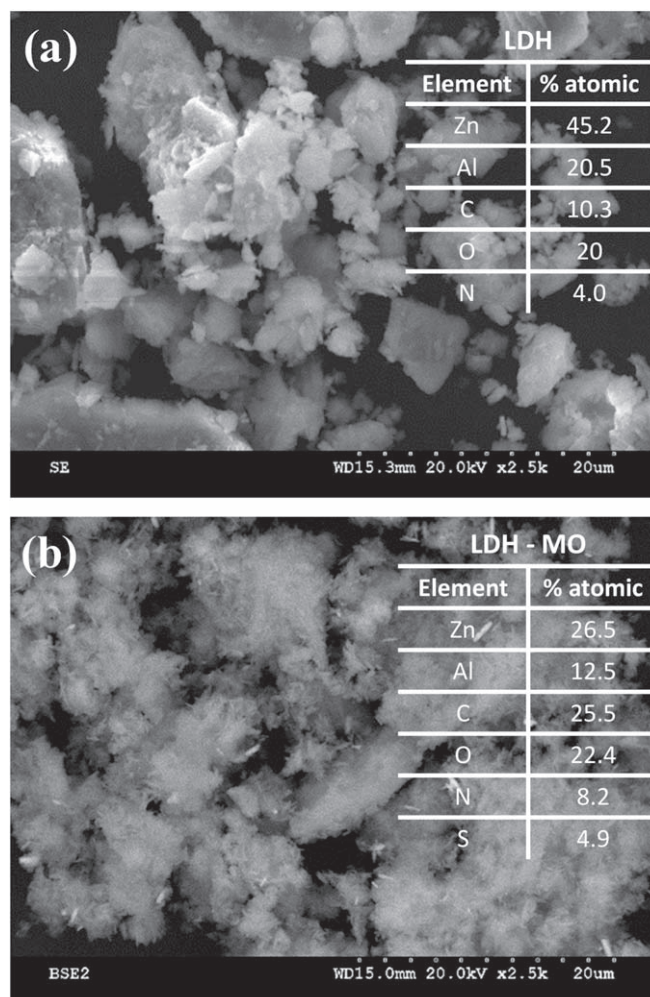


**Figure 2.** SEM micrograph of the synthesized (a) LDH and (b) LDH-MO and the elements detected by EDS in the inset of the micrographs.

than the current density of the cyclic voltammetry of iron without an aggressive medium and without LDH). Figure 3(a) presents the voltammograms from  $E_{corr}$  to more positive potential values of the various LDH coatings and bare iron. All LDH inhibit the pitting corrosion process since in all cases, the pitting potential in the LDH samples is more positive than that of the iron cast. In addition, nonlinear dependence of the inhibition properties on the concentration of LDH is identified, and the best performance is realized when the iron was immersed in LDH  $2 \text{ g l}^{-1}$  with an  $E_{pit}$  value that is close to  $-0.35 \text{ V}$  versus Ag/AgCl. This nonlinear dependence has also been reported recently in LDH-epoxy composites [44]. The inhibition of the pitting corrosion process arises from the anion exchange of  $\text{NO}_3^-$  from the LDH inter lamellar space to the surface solution, while chloride ions remain trapped in the LDH in the opposite direction [44–47]. This decrease in the ion chloride concentration on the surface moves the pitting potential to more positive values, thereby inhibiting the corrosion process since the  $E_{pit}$  potential depends on the chloride surface concentration [48]. The  $E_{pit}$  evolution during the exposure time was measured for 72 h for LDH  $2 \text{ g l}^{-1}$  with independent samples. Figure 3(b) shows the  $E_{pit}$  evolution of LDH  $2 \text{ g l}^{-1}$  and bare iron. The  $E_{pit}$  of bare iron remains constant at a negative value ( $0.550 \text{ V}$  versus Ag/AgCl) throughout the exposure time; hence, the active pitting corrosion process is occurring. However, the  $E_{pit}$  evolution for the LDH samples decreases during the first day, and up to this time, the  $E_{pit}$  remains constant at a more positive value than that for the bare iron ( $0.450 \text{ V}$  versus Ag/AgCl). This more positive  $E_{pit}$  supports the inhibitory effect of the LDH layers via the trapping of chloride ions. The same experimental tests were conducted with LDH-MO. In this case, the pitting corrosion process is inhibited, and the anodic currents are below the threshold current for pitting corrosion ( $0.001 \text{ A cm}^{-2}$ ).

According to the anodic curves (Figure 4) for both exposure times, while the use of LDH delays the initiation of the pitting corrosion process, with LDH-MO, the pitting corrosion process is not detected. The bare iron and iron that is covered with LDH present almost parallel anodic polarization curves, which correspond for both cases to the pitting corrosion process. However, LDH-MO shows passive behaviour, which indicates the absence

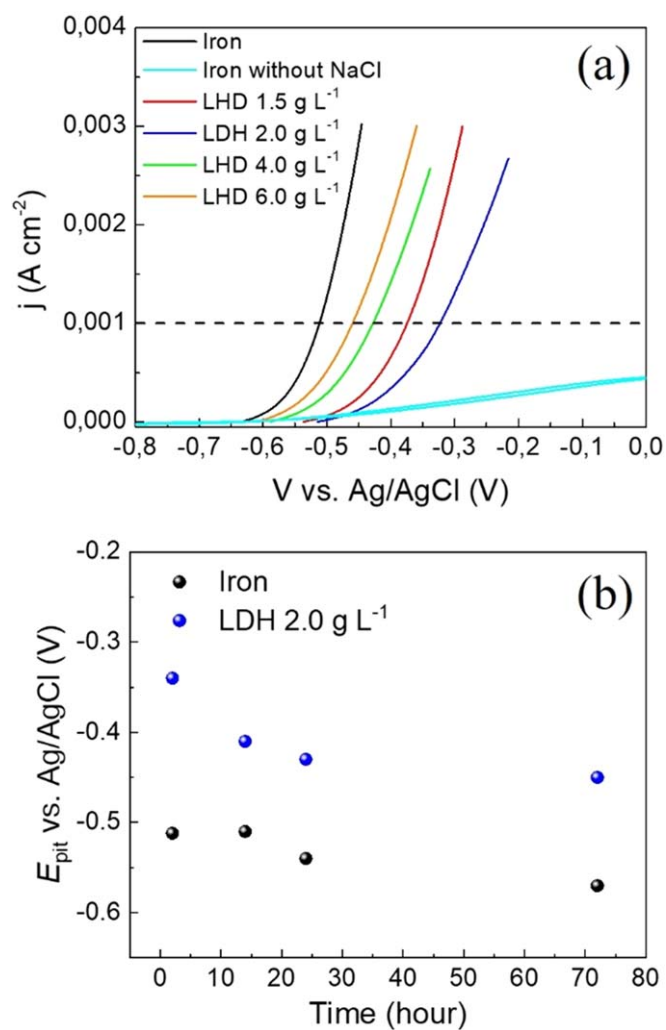


**Figure 3.** (a) Pitting corrosion potential evolution in LDH and bare iron. Scan rate 0.005 Vs<sup>-1</sup>, 3.5% NaCl. (b) Pitting corrosion potential determination by polarization curves in LDH and bare iron. Scan rate 0.005 Vs<sup>-1</sup>, 3.5% NaCl.

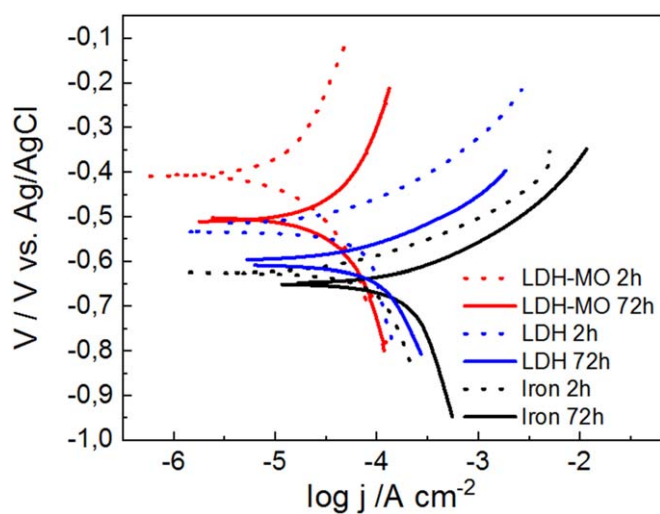
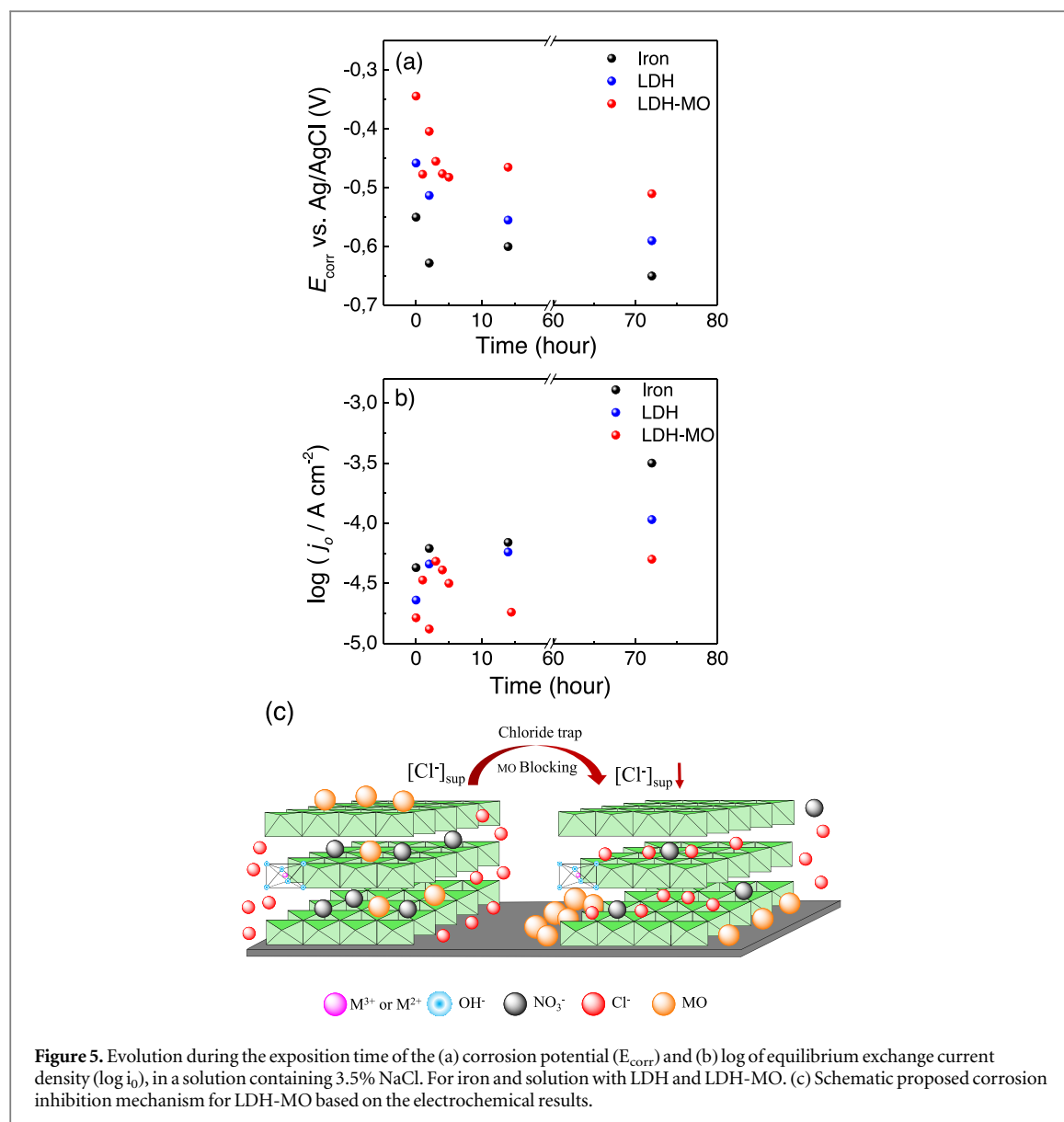


**Figure 4.** Polarization curves at 2 and 72 h of immersion for iron with LDH, LDH-MO at 2 g l<sup>-1</sup> and iron base in 3.5% NaCl, scan rate 0.005 Vs<sup>-1</sup>. The polarization curve was started from the open circuit potential ( $E_{ocp}$ ) to  $\pm 300$  mV versus  $E_{ocp}$  with independent samples.





of an active corrosion process. According to the cathodic polarization curves, the behaviours differ among the exposure times and samples. At short times (dashed lines), the three samples undergo the oxygen reduction reaction (ORR) with similar activity. Nevertheless, at the end of the experiment, the ORR is delayed in the LDH-MO sample, while LDH and bare iron present similar behaviour at more positive currents. The inhibition of cathodic and anodic reactions implies that the inhibition of LDH-MO follows a mixed inhibition mechanism with physical adsorption of MO on the iron surface, which blocks the iron sites for the ORR and corrosion. A similar inhibition mechanism has been proposed for azo dyes in acidic media [49]. In addition, a possible contribution of the chloride trapping effect of the LDH matrix in the inhibition process must be considered.

The evolutions of the corrosion potential ( $E_{\text{corr}}$ ) and the exchange density current ( $\log i_0$ ) over the immersion time are presented in figure 5. The bare iron samples show the highest current densities and lowest  $E_{\text{corr}}$ , which are characteristic of an intense pitting corrosion process. However, the presence of LDH and LDH-MO reduces the exchange current density. As shown in figure 5(b), during the first 2 h of exposure, the three samples present similar behaviour with a constant increase in the current density.

Up to this time, the current density of bare iron increases approximately one order of magnitude during the test. However, the current densities of LDH increase more slowly and remain stable due to the decrease of the chloride concentration on the metal surface. The LDH-MO system presents different behaviour: after the first two hours, the current density decreases, which could be associated with the physical adsorption process of MO on the iron surface. Due to the synergistic effect of chloride trapping and MO adsorption, the LDH-MO samples show the best inhibition efficiency, with a reduction in the exchange current density of one order of magnitude. Figure 5(c) shows a schematic diagram of the corrosion inhibition for LDH and LDH-MO, which is based on the

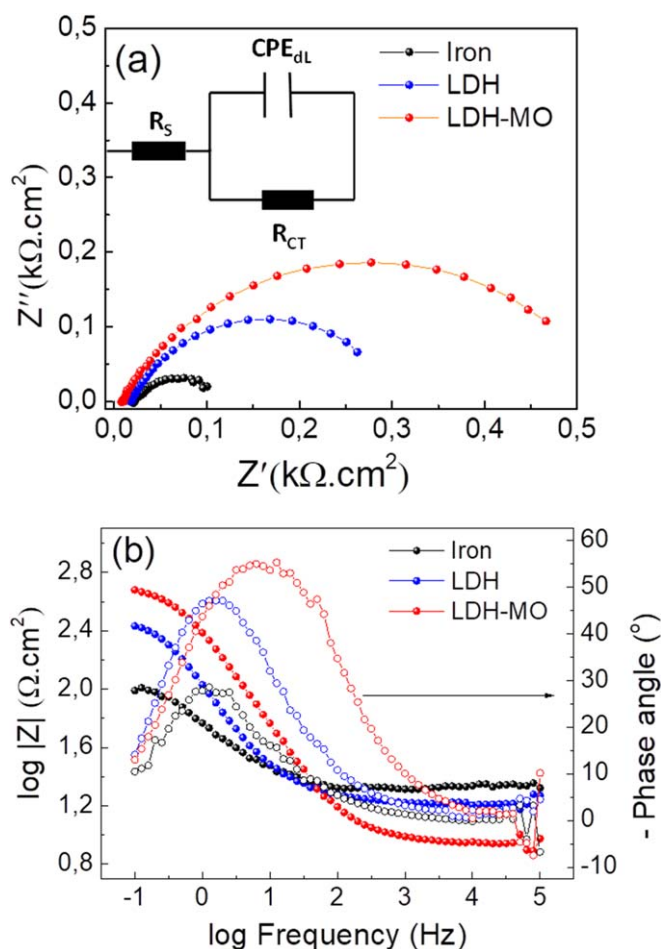


**Figure 6.** (a) Nyquist plot and (b) Bode plot obtained from the iron electrode determined after 2h of immersion in (black) 3.5% NaCl solution without inhibitor, (blue) solution with LDH ( $2 \text{ gl}^{-1}$ ) and (red) solution with LDH-MO ( $2 \text{ gl}^{-1}$ ).

electrochemical results. These results show that the inhibition of corrosion with LDH is due to the entrapment of chloride anion and the release of nitrate and MO, respectively. This reduction in the chloride concentration on the iron surfaces produces a decrease in the corrosion rate.

The corrosion-inhibiting efficiency calculated from polarization curve ( $\eta_{pc}$ ) can be calculated as follows:

$$\eta_{pc} = \frac{i_{corr} - i'_{corr}}{i_{corr}} \times 100$$

Where  $i_{corr}$  and  $i'_{corr}$  are the corrosion current densities of the substrate in the system in the absence and presence of the inhibitors anion, respectively. The values obtained by LDH and LDH-MO are 80 and 90%, respectively. Also, the corrosion-inhibiting efficiency has been calculated for MO in solution, being its value of 87% close to the value found for the LDH-MO.

To confirm the above results obtained by polarization measurements, similar tests were carried out by electrochemical impedance spectroscopy at short times. Figures 6(a) and (b) show iron Nyquist and Bode diagrams performed both at OCP in absence and presence of LDHs. The Nyquist plots present a non-ideal semicircle, which is attributed to the non-ideality of the metal surface [50].

The Nyquist plots represent the characteristic depressed semicircles with their centers lying under the real  $x$ -axis, suggesting that the electrochemical process is charge-transfer controlled. On the other hand, the corresponding Bode plots showed in figure 6(b) confirm the presence of only one constant time due to charge transfer phenomenon at the interface electrolyte/surface electrode. The EIS data were fitted using an equivalent circuit of one relaxation times (inset figure 6(a)). Where  $R_s$  is the electrolyte resistance,  $R_{ct}$  the resistance of charger transfer and  $CPE_{dl}$  the capacity of the double layer. The chi-square ( $\chi^2$ ) values were calculated to determine the quality of the equivalent circuit fitting. A values of  $\chi^2 < 10^{-3}$  were obtained for all data, indicating a good agreement with the experimental data. The values of  $R_{ct}$  obtained were 120, 313, 558  $\Omega \text{ cm}^2$  for iron in solution of NaCl in absence of LDH, in presence of LDH and in presence of LDH-MO, respectively (with a standard deviation range between the 2 and 6%). These values show a higher inhibiting performance of LDH-

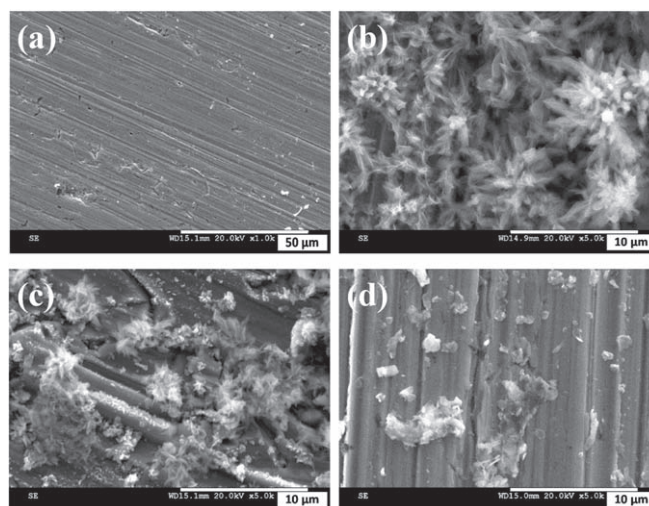


**Figure 7.** SEM micrograph (a) iron, (b) iron after two hours in 3.5% NaCl, (c) iron in solution with 3.5% NaCl + LDH 2  $\text{gl}^{-1}$  after two hours and (d) iron in solution with 3.5% NaCl + 2  $\text{gl}^{-1}$  LDH-MO after two hours.

MO in comparison to LDH. The inhibition efficiency obtained with LDH-MO tests is comparable with the obtained using ZnAl-vanadate LDH and MgAl-vanadate LDH reported by Zheludkevich *et al* [2]. These results are similar to those found using the polarization curves and this behavior has also been observed in other studies [31].

Figure 7 shows SEM images of the iron surface before (figure 7(a)) and after (figure 7(b)) the test. The bare iron surface is smooth prior to exposure to 3.5% NaCl and is covered by corrosion products after the tests. The LDH surface after the tests (figure 7(c)) is smoother, with the presence of isolated pits and small corrosion products. In contrast, the iron that was immersed in LDH-MO (figure 7(d)) shows a smooth surface that is highly similar to that of the bare iron, and only tiny pits are detected on the surface. These pits could be associated with the metastable pits that developed during the first hours of exposure before MO adsorption, thereby supporting the  $\log j_o$  measures that are presented in figure 5(b).

## 4. Conclusions

The synthesis and corrosion inhibition behaviours of LDH and LDH-MO were evaluated in a 3.5% NaCl solution. The XRD study shows the successful synthesis of the LDH and LDH-MO compounds. The characterization showed that MO is present in the interlamellar space and could also be adsorbed onto the LDH surface. Based on the experimental results, the use of LDH-MO as an inhibitor yields better results than the use of LDH due to the dual inhibitor effect, the chloride trapping on the LDH, and the MO adsorption on the iron surface. According to the optimization of LDH, the best performance is realized with 2  $\text{gl}^{-1}$  solution concentration, and its anticorrosive performance decreases as the concentration is increased. This concentration of LDH and LDH-MO inhibited the pitting corrosion process for 72 h. LDH-MO presents the highest anticorrosive properties with an exchange current decrease of one order of magnitude with respect to iron. Based on these results, additional investigation is necessary to optimize the amount of the MO inhibitor for technical and practical applications in polymer coatings.

## Acknowledgments

The Spanish Ministry of Economy and Competitiveness funded this research under project PGC2018-095642-B-I00.

## Data availability statement

All data that support the findings of this study are included within the article (and any supplementary files).



## ORCID iDs

O Benali  <https://orcid.org/0000-0002-7638-6478>

E Mazarío  <https://orcid.org/0000-0001-8235-0087>

P Herrasti  <https://orcid.org/0000-0003-1067-0780>

## References

- [1] Walter G W 1986 A critical review of the protection of metals by paints *Corros. Sci.* **26** 27–38
- [2] Zheludkevich M L, Poznyak S K, Rodrigues L M, Raps D, Hack T, Dick L F, Nunes T and Ferreira M G S 2010 Active protection coatings with layered double hydroxide nanocontainers of corrosion inhibitor *Corros. Sci.* **52** 602–11
- [3] Abdullayev E, Price R, Shchukin D and Lvov Y 2009 Halloysite tubes as nanocontainers for anticorrosion coating with benzotriazole *ACS Appl. Mater. Interfaces* **1** 1437–43
- [4] Dong B, Ding W, Qin S, Han N, Fang G, Liu Y, Xing F and Hong S 2018 Chemical self-healing system with novel microcapsules for corrosion inhibition of rebar in concrete *Cem. Concr. Compos.* **85** 83–91
- [5] Noiville R, Jaubert O, Gressier M, Bonino J-P, Taberna P-L, Fori B and Menu M-J 2018 Ce(III) corrosion inhibitor release from silica and boehmite nanocontainers *Mater. Sci. Eng. B* **229** 144–54
- [6] Yeganeh M, Omid M, Mortazavi S H H, Etemad A, Nazari M H and Marashi S M 2020 Chapter 15—application of mesoporous silica as the nanocontainer of corrosion inhibitor *Corrosion Protection at the Nanoscale Micro and Nano Technologies* ed S Rajendran, T A N H Nguyen, S Kakooei, M Yeganeh and Y Li (Amsterdam: Elsevier) 275–94
- [7] Zheludkevich M L, Serra R, Montemor M F, Yasakau K A, Salvado I M M and Ferreira M G S 2005 Nanostructured sol–gel coatings doped with cerium nitrate as pre-treatments for AA2024–T3 Corrosion protection performance *Electrochim. Acta* **51** 208–17
- [8] Xu D, Lou C, Huang J, Lu X, Xin Z and Zhou C 2019 Effect of inhibitor-loaded halloysite nanotubes on active corrosion protection of polybenzoxazine coatings on mild steel *Prog. Org. Coatings* **134** 126–33
- [9] Shchukin D G, Lamaka S V, Yasakau K A, Zheludkevich M L, Ferreira M G S and Möhwald H 2008 Active anticorrosion coatings with halloysite nanocontainers *J. Phys. Chem. C* **112** 958–64
- [10] Tedim J, Poznyak S K, Kuznetsova A, Raps D, Hack T, Zheludkevich M L and Ferreira M G S 2010 Enhancement of active corrosion protection via combination of inhibitor-loaded nanocontainers *ACS Appl. Mater. Interfaces* **2** 1528–35
- [11] Shchukin D G, Zheludkevich M, Yasakau K, Lamaka S, Ferreira M G S and Möhwald H 2006 Layer-by-layer assembled nanocontainers for self-healing corrosion protection *Adv. Mater.* **18** 1672–8
- [12] Xu M and Wei M 2018 Layered double hydroxide-based catalysts: recent advances in preparation, structure, and applications *Adv. Funct. Mater.* **28** 1802943
- [13] Wang Q and O'Hare D 2012 Recent advances in the synthesis and application of layered double hydroxide (LDH) nanosheets *Chem. Rev.* **112** 4124–55
- [14] Guo X, Zhang F, Evans D G and Duan X 2010 Layered double hydroxide films: synthesis, properties and applications *Chem. Commun.* **46** 5197–210
- [15] Peng F, Wang D, Tian Y, Cao H, Qiao Y and Liu X 2017 Sealing the pores of PEO coating with Mg–Al layered double hydroxide: enhanced corrosion resistance, cytocompatibility and drug delivery ability *Sci. Rep.* **7** 8167
- [16] Alibakhshi E, Ghasemi E, Mahdavian M, Ramezanzadeh B and Farashi S 2017 Active corrosion protection of Mg–Al–PO<sub>4</sub>–LDH nanoparticle in silane primer coated with epoxy on mild steel *J. Taiwan Inst. Chem. Eng.* **75** 248–62
- [17] Marappa S and Kamath P V 2018 NO<sub>2</sub><sup>−</sup> and SCN<sup>−</sup>-intercalated layered double hydroxides: structure and orientation of anions in the interlayer gallery *Bull. Mater. Sci.* **41** 26
- [18] Wen T, Yan R, Wang N, Li Y, Chen T and Ma H 2020 PPA-containing layered double hydroxide (LDH) films for corrosion protection of a magnesium alloy *Surf Coatings Technol.* **383** 125255
- [19] Li L-X, Xie Z-H, Fernandez C, Wu L, Cheng D, Jiang X-H and Zhong C-J 2020 Development of a thiophene derivative modified LDH coating for Mg alloy corrosion protection *Electrochim. Acta* **330** 135186
- [20] Cao Y, Zheng D, Luo J, Zhang F, Dong S, Pan J and Lin C 2019 Insight into the fabrication of ZnAl layered double hydroxides intercalated with organic anions and their corrosion protection of steel reinforced concrete *J. Electrochem. Soc.* **166** C617–23
- [21] Poznyak S K, Tedim J, Rodrigues L M, Salak A N, Zheludkevich M L, Dick L F P and Ferreira M G S 2009 Novel inorganic host layered double hydroxides intercalated with guest organic inhibitors for anticorrosion applications *ACS Appl. Mater. Interfaces* **1** 2353–62
- [22] Serdechnova M, Mohedano M, Kuznetsov B, Mendis C L, Starykevich M, Karpushenkov S, Tedim J, Ferreira M G S, Blawert C and Zheludkevich M L 2017 PEO coatings with active protection based on *in-situ* formed LDH-nanocontainers *J. Electrochem. Soc.* **164** C36–45
- [23] Tedim J, Zheludkevich M L, Salak A N, Lisenkov A and Ferreira M G S 2011 Nanostructured LDH-container layer with active protection functionality *J. Mater. Chem.* **21** 15464–70
- [24] Ishizaki T, Chiba S, Watanabe K and Suzuki H 2013 Corrosion resistance of Mg–Al layered double hydroxide container-containing magnesium hydroxide films formed directly on magnesium alloy by chemical-free steam coating *J. Mater. Chem. A* **1** 8968–77
- [25] Zhang G, Wu L, Tang A, Chen X-B, Ma Y, Long Y, Peng P, Ding X, Pan H and Pan F 2018 Growth behavior of MgAl-layered double hydroxide films by conversion of anodic films on magnesium alloy AZ31 and their corrosion protection *Appl. Surf. Sci.* **456** 419–29
- [26] Wu B, Zuo J, Dong B, Xing F and Luo C 2019 Study on the affinity sequence between inhibitor ions and chloride ions in MgAl layer double hydroxides and their effects on corrosion protection for carbon steel *Appl. Clay Sci.* **180** 105181
- [27] Zuo J, Wu B, Luo C, Dong B and Xing F 2019 Preparation of MgAl layered double hydroxides intercalated with nitrite ions and corrosion protection of steel bars in simulated carbonated concrete pore solution *Corros. Sci.* **152** 120–9
- [28] Okeniyi J O, Omotosho O A, Ajayi O O and Loto C A 2014 Effect of potassium-chromate and sodium-nitrite on concrete steel-rebar degradation in sulphate and saline media *Constr. Build. Mater.* **50** 448–56
- [29] Chen J, Song Y, Shan D and Han E-H 2013 Modifications of the hydrotalcite film on AZ31 Mg alloy by phytic acid: the effects on morphology, composition and corrosion resistance *Corros. Sci.* **74** 130–8
- [30] Alibakhshi E, Ghasemi E, Mahdavian M and Ramezanzadeh B 2017 Fabrication and characterization of layered double hydroxide/silane nanocomposite coatings for protection of mild steel *J. Taiwan Inst. Chem. Eng.* **80** 924–34

- [31] Alibakhshi E, Ghasemi E, Mahdavian M and Ramezanzadeh B 2017 A comparative study on corrosion inhibitive effect of nitrate and phosphate intercalated Zn–Al- layered double hydroxides (LDHs) nanocontainers incorporated into a hybrid silane layer and their effect on cathodic delamination of epoxy topcoat *Corros. Sci.* **115** 159–74
- [32] Alibakhshi E, Ghasemi E, Mahdavian M, Ramezanzadeh B and Farashi S 2016 Fabrication and characterization of PO43–intercalated Zn–Al- layered double hydroxide nanocontainer *J. Electrochem. Soc.* **163** C495–505
- [33] Xu J, Song Y, Zhao Y, Jiang L, Mei Y and Chen P 2018 Chloride removal and corrosion inhibitions of nitrate, nitrite-intercalated MgAl layered double hydroxides on steel in saturated calcium hydroxide solution *Appl. Clay Sci.* **163** 129–36
- [34] Ni Z-M, Xia S-J, Wang L-G, Xing F-F and Pan G-X 2007 Treatment of methyl orange by calcined layered double hydroxides in aqueous solution: adsorption property and kinetic studies *J. Colloid Interface Sci.* **316** 284–91
- [35] Lyu H, Hu K, Fan J, Ling Y, Xie Z and Li J 2020 3D hierarchical layered double hydroxide/carbon spheres composite with hollow structure for high adsorption of dye *Appl. Surf. Sci.* **500** 144037
- [36] Clark I, Smith J, Gomes R L and Lester E 2019 Continuous synthesis of Zn2Al-CO3 layered double hydroxides for the adsorption of reactive dyes from water *J. Environ. Chem. Eng.* **7** 103175
- [37] Shamim M and Dana K 2018 Efficient removal of Evans blue dye by Zn–Al–NO3 layered double hydroxide *Int. J. Environ. Sci. Technol.* **15** 1275–84
- [38] Ebenso E E and Oguzie E E 2005 Corrosion inhibition of mild steel in acidic media by some organic dyes *Mater. Lett.* **59** 2163–5
- [39] Oguzie E E 2004 Influence of halide ions on the inhibitive effect of congo red dye on the corrosion of mild steel in sulphuric acid solution *Mater. Chem. Phys.* **87** 212–7
- [40] Li X, Deng S and Fu H 2010 Inhibition effect of methyl violet on the corrosion of cold rolled steel in 1.0M HCl solution *Corros. Sci.* **52** 3413–20
- [41] Pan D, Zhang H, Zhang T and Duan X 2010 A novel organic–inorganic microhybrids containing anticancer agent doxifluridine and layered double hydroxides: structure and controlled release properties *Chem. Eng. Sci.* **65** 3762–71
- [42] Darmograi G, Prelot B, Layrac G, Tichit D, Martin-Gassin G, Salles F and Zajac J 2015 Study of adsorption and intercalation of orange-type dyes into Mg–Al layered double hydroxide *J. Phys. Chem. C* **119** 23388–97
- [43] Morimoto K, Tamura K, Iyi N, Ye J and Yamada H 2011 Adsorption and photodegradation properties of anionic dyes by layered double hydroxides *J. Phys. Chem. Solids* **72** 1037–45
- [44] Xu J, Tan Q and Mei Y 2020 Corrosion protection of steel by Mg–Al layered double hydroxides in simulated concrete pore solution: Effect of SO42- *Corros. Sci.* **163** 108223
- [45] Deip A R, Leal D A, Sakae G H, Maia F, Berton M A C, Ferreira M G S and Marino C E B 2020 Performance of commercial LDH traps for chloride ion in a commercial corrosion protection primer for petrochemical industry *Corros. Eng. Sci. Technol.* **55** 66–74
- [46] Lv L, He J, Wei M, Evans D G and Duan X 2006 Uptake of chloride ion from aqueous solution by calcined layered double hydroxides: equilibrium and kinetic studies *Water Res.* **40** 735–43
- [47] Goh K-H and Lim T-T 2010 Influences of co-existing species on the sorption of toxic oxyanions from aqueous solution by nanocrystalline Mg/Al layered double hydroxide *J. Hazard. Mater.* **180** 401–8
- [48] Ergun M and Turan A Y 1991 Pitting potential and protection potential of carbon steel for chloride ion and the effectiveness of different inhibiting anions *Corros. Sci.* **32** 1137–42
- [49] Palanisamy K, Kannan P and Sekar A 2018 Evaluation of chromotrope FB dye as corrosion inhibitor using electrochemical and theoretical studies for acid cleaning process of petroleum pipeline *Surfaces and Interfaces* **12** 50–60
- [50] Attou A, Tourabi M, Benikdes A, Benali O, Ouici H B, Benhiba F, Zarrouk A, Jama C and Bentiss F 2020 Experimental studies and computational exploration on the 2-amino-5-(2-methoxyphenyl)-1,3,4-thiadiazole as novel corrosion inhibitor for mild steel in acidic environment *Colloids Surfaces A Physicochem. Eng. Asp.* **604** 125320